The Semicrystalline Morphology of Poly(ether−ether−ketone) Blends with Poly(ether−imide)

Alain M. Jonas* and Dimitri A. Ivanov‡

Unité de Chimie et de Physique des Hauts Polymères, Université Catholique de Louvain, Place Croix du Sud, 1, B-1348 Louvain-la-Neuve, Belgium

Do Y. Yoon*

IBM Research Division, Almaden Research Center, 650 Harry Road, San Jose, California 95120

Received July 31, 1997; Revised Manuscript Received May 15, 1998

ABSTRACT: The microstructure of cold-crystallized poly(ether−ether−ketone)/poly(ether−imide) (PEEK/PEI) blends has been investigated by a combination of wide- and small- angle X-ray scattering (SAXS), dielectric spectroscopy, and transmission electron microscopy. Both SAXS and dielectric spectroscopy indicate that most PEI is excluded from interlamellar regions and segregates essentially into interfibrillar regions upon crystallization. Interlamellar inclusion was found to be limited to low PEI levels. Transmission electron microscopy (TEM) observations on stained thin sections from bulk samples confirm these conclusions. The restricted character of the interlamellar inclusion of PEI is probably due to a more ordered structure of noncrystalline regions near PEEK crystal surfaces. In addition, our results on PEEK/PEI blends corroborate the model of cold-crystallized pure PEEK which consists of thin lamellar crystals separated by thicker noncrystalline interlayers that are grouped into stacks of limited coherence and uniformly fill the entire sample volume without any separate amorphous pockets or gaps.

1. Introduction

Poly(ether−ether−ketone) (PEEK)[1] is a typical aromatic semicrystalline polymer which is comprised of a fully para-aromatic backbone arrangement. It is noted for high performance properties among which are excellent thermal and chemical stability, the absence of polymorphic transitions, and an extremely large temperature interval of crystallization. The semicrystalline microstructure of PEEK has been much discussed recently, owing to a difference between authors in the interpretation of the small-angle X-ray scattering (SAXS) results for this polymer.[2,3] This problem affects directly the interpretation of the much-debated multiple endothermic behavior exhibited by isothermally crystallized PEEK.[2−11]

In short, the proposed microstructural models can be divided into two groups. The first model is in essence a three-phase model, wherein thick lamellar crystals (about 70−120 Å) separated by thinner amorphous interlayers (about 30−40 Å) pack into stacks of finite size, these stacks being separated by large purely amorphous PEEK regions.[3,11−13] The large amorphous gaps represent a significant fraction of the polymer (up to 50% according to this model). Different variants of this model have been presented; we refer the reader to ref 3 for details. These models are often referred as "finite stack models";[3] however, we will call them "heterogeneous models" herein.

The second model is primarily a two-phase model, wherein the sample is homogeneously filled with stacks of thin lamellae alternating with thicker amorphous interlayers.[2,4,14−16] This model has been called by its opponents as an "infinite stack model",[3] because no large amorphous gaps are considered to exist in the crystallized polymer. However, the rapid loss of correlation in the positions of lamellae as a function of their distance leads to an effective cutoff length for coherent scattering, so that the word "infinite" becomes misleading. Hence we will designate this model as "homogeneous model". This model has been successfully used to explain synchrotron X-ray scattering data obtained during complex thermal treatments on various PEEK samples,[2,15,16] as well as to correlate the variations of the glass transition of PEEK with the thickness of amorphous interlayers.[14]

Previously, we have presented arguments in favor of the homogeneous model.[2] We also suggested that large differences in the thermal treatments of investigated samples could be the reason for the disagreement between the proposed models.[2] In this regard, recent studies by Fougnies et al.[15,16] tend to indicate that the applicability of heterogeneous models is restricted to samples melt-crystallized near 340 °C, in the vicinity of the main melting endotherm of PEEK. It is interesting to note that the proponents of the heterogeneous models have precisely devoted their efforts to samples melt-crystallized at rather high temperatures, usually above 300 °C, in a temperature range of little practical relevance. At these elevated temperatures, the chemical nature of PEEK samples could become more heterogeneous due to slow degradation, which may then be the reason for the presence of amorphous gaps.

Therefore, the first aim of the present paper is to definitively test the validity of the homogeneous model of lamellar microstructure for PEEK samples crystallized below 300 °C. This will be achieved by taking advantage of the characteristics of PEEK/poly(ether−imide) (PEI)[1] blends. These blends belong to the class of semicrystalline/amorphous miscible polymer blends. These blends are made of two polymers miscible in the amorphous melt state; upon cooling from the melt or

* To whom correspondence should be addressed.
‡ Current address: Unité de Physique des Polyméres, Departement de Physique, Université Libre de Bruxelles, CP223, Boulevard du Triomphe, 1050 Brussels, Belgium.

S0024-9297(97)01160-1 CCC: $15.00
Published on Web 07/24/1998

heating from the supercooled glass, one of the component (PEEK) crystallizes, thereby rejecting the other noncrystallizable component (PEI) into amorphous regions. Since the different microstructural models differ strongly in the way amorphous PEEK is distributed in the semicrystalline structure, the ability to probe these regions through the characteristics of PEI provides a very powerful tool to resolve the problem. In our investigation, we obtained a diverse set of experimental results on PEEK/PEI blends, using transmission electron microscopy (TEM), wide- and small-angle X-ray scattering (WAXS and SAXS), and dielectric spectroscopy.

For semicrystalline/amorphous miscible polymer blends, the rejection of the noncrystallizable component upon crystallization can a priori occur in three modes:[17] (1) interlamellar, where it is located in the amorphous regions between lamellar crystals; (2) interfibrillar, where it is located between bundles of lamellae (or fibrils) inside the spherulites; (3) interspherulitic, where it is excluded from the spherulites, giving rise to a morphology consisting in spherulites dispersed in a sea of the noncrystallizable component. It is difficult to predict the mode of segregation for a given blend. The use of a kinetic parameter has been proposed,[18] but this phenomenological theory has not yet been completely validated. In this regard, PEEK/PEI blends have already been investigated in the literature.[12,19−26] Poly(ether−imide) has been reported to segregate only interfibrillarly or interspherulitically upon crystallization of PEEK.[12,19,20,24] However, we have shown in a preliminary report[26] the occurrence of partial PEI interlamellar inclusion for cold-crystallized blends, and this has been corroborated by recent dielectric relaxation studies for melt-crystallized blends by Bristow and Kalika.[25] A second aim of this paper is thus to clarify the mode of segregation of PEI in the blends, using results obtained by different techniques on identical bulk samples, to obtain a consistent picture.

The third aim of this paper logically follows the finding of the second objective: it is to get information on the nature of PEEK noncrystalline amorphous interlamellar regions from the miscibility characteristics of PEI in these regions. For some other semicrystalline blends, it has indeed been shown that the noncrystallizable polymer is rejected not only from the crystals of the crystallizing polymer but also from an interphase region at the surface of the crystals.[27,28] Theoretical considerations have rationalized the concept of compositional interphase in term of a balance between the interaction energy due to the contacts between the two components (interaction parameter χ), and the "urgent" need to dissipate the order of the polymer segments emerging from the crystal surfaces.[29] The picture was further refined[30] by incorporating terms taking into account the tight-fold energy (E_η). These studies predict the existence at the crystal surface of a transition region in which the crystalline order progressively dissipates, which is in agreement with a series of experimental findings by Mandelkern et al.[31] The thickness of this partially ordered interphase mainly depends on E_η, for example. The theory also predicts the existence of a compositional interphase whose thickness depends on χ and E_η.

Experimental Section

Polymer Samples. PEEK powder (Victrex 150P) was received from ICI. Molecular masses determined by size exclusion chromatography are 10 300 for M_n and 26 800 for M_w, respectively.[32,33] PEI powder (Ultem 1000) was supplied by General Electric. The molecular mass of PEI has been reported to be 14 000 for M_w.[34] The powders were dried overnight at 150 °C under vacuum before processing.

Blends. The polymers were mixed for 10 min in the molten state in a Brabender mixer operated at 380 °C under a nitrogen atmosphere. The pellets were compression-molded at 400 °C for 10 min in vacuum bags, to obtain films of about 400 μm thickness. These conditions were selected in order to avoid branching of the PEEK polymer during processing, as detailed elsewhere.[32] The films were directly quenched from 400 °C into water at room temperature. The quenched films were transparent with no voids. Wide-angle X-ray diffraction patterns showed no trace of crystallinity in these films; we also confirmed the absence of preferential orientation in the samples, by taking X-ray photographs for three different orientations of the sheets in the beam. The films were crystallized for 9.5 h by placing them in a nitrogen-filled oven previously set at the desired temperature T_c in the range of 200−280 °C. The temperature stability of the oven was measured to be ±3 °C.

Wide-Angle X-ray Scattering. Wide-angle X-ray patterns of the amorphous and annealed sheets were taken in reflection between 5 and 100° (2θ) with a Siemens diffractometer mounted on a rotating anode generator (Cu Kα). The photons were discriminated by energy (cooled semiconductor detector). The settings of the discrimination window allowed the detection of the coherently scattered radiation, and all the incoherently scattered (Compton) radiation in the angular range of our experiments. The spectra were corrected for absorption and geometric effects and then scaled to absolute units as described elsewhere.[35] After subtraction of the incoherent scattering, the data were used to compute absolute values of crystallinity by using Ruland's method.[36] The method requires one to separate crystalline peaks from the amorphous halo in the spectra of the semicrystalline samples. Above $s = (2 \sin \theta)/\lambda = 0.3$ Å^{-1} (with λ the X-ray wavelength and 2θ the diffraction angle), the scattering of the pure amorphous samples was used as a basis to perform this separation, using Vonk's procedure;[37] below this s value, the data were fit to a combination of Pearsons type VII distributions of third order[38] representing the crystalline peaks and a sum of broad Gaussians representing the amorphous halo. This treatment is necessary because the amorphous halos of semicrystalline samples and of pure amorphous samples are quite different in the low s range. Typical computed amorphous halos are shown in Figure 1. We adapted Ruland's equations for our case where the composition of the amorphous regions differs from that of the crystals (the correction is rather small, given the similarity of the average mass per atom for PEEK and PEI). The analysis also requires a disorder factor ($D(s)$ as defined in ref 36) which depends on the kind of distortions existing in the crystals. Given the strong variations of crystal density with annealing conditions,[2,39] we selected the expression pertaining to a dominance of distortions of the second kind (paracrystallinity)

$$D(s) = \frac{2 \exp(-ks^2)}{1 + \exp(-ks^2)}, \qquad (1)$$

where k is a parameter proportional to the average width of the distributions of interplanar distances in the crystal[40] (smaller k's correspond to decreasing disorder). Finally, instead of using the parabolic approximation of Vonk[37] to fit the processed data, we used exact theoretical expressions.

Small-Angle X-ray Scattering. Measurements were performed on beamline I-4 at the Stanford Synchrotron Radiation Laboratory (SSRL). The data were corrected for parasitic scattering and normalized to unit incident intensity and unit effective thickness.[41] No desmearing was performed, given the high collimation of the beam and its very small cross-section. Other corrections are indicated where appropriate.

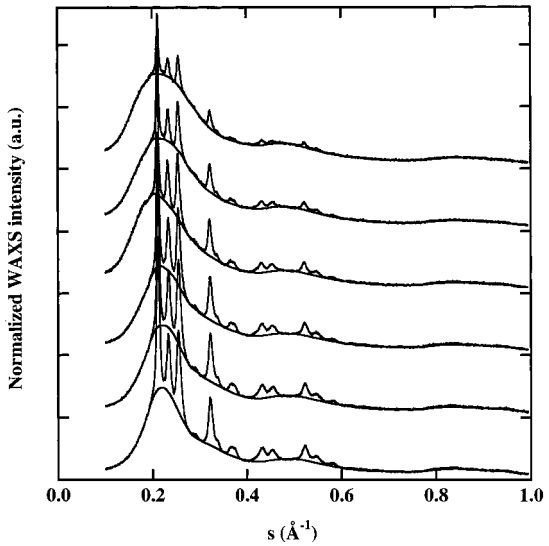

Figure 1. Wide-angle X-ray patterns of PEEK/PEI blends annealed for 9.5 h at 280 °C, with PEI content, from bottom to top of 0, 10, 20, 40, 60, and 80 wt %. The amorphous halos computed for the Ruland analysis are also shown in this figure (the curves are displaced vertically for clarity).

Transmission Electron Microscopy (TEM). Ultrathin sections of bulk specimens (approximately 50−100 nm thick) were obtained at room temperature using a Reichert FCS microtome fitted with a diamond knife. The staining solution was prepared by dissolving 0.1 g of ruthenium trichloride hydrate (Janssen Chimica) in 5.0 mL of 27.3% aqueous sodium hypochlorite (Aldrich). The mixture was used immediately after the preparation as it deteriorates with time. The microtomed sections, supported on 400 mesh TEM grids, were exposed to the vapors of the ruthenium/hypochlorite mixture in a desiccator containing several milliliters of solution for different periods depending on the sample. These conditions ensure a rapid staining of the PEEK fraction while leaving virtually unaffected PEI-rich regions. PEEK thus appears black in our TEM micrographs, while PEI is white. Stained and unstained sections were observed in a Philips EM 301 transmission electron microscope operating at 80 kV. More experimental details can be found in ref 42.

Dielectric Spectroscopy. Guarded measurements were performed at seven frequencies between 200 Hz and 100 kHz with a Hewlett-Packard HP4274A bridge. The gold electrodes were vacuum deposited with a patterned mask. The samples were sandwiched between insulated copper plates to ensure lateral homogeneity of temperature. Temperature was measured with a thin thermocouple located on the sample outside the measuring electrodes. Samples were first dried in the dielectric cell at 100 °C (below T_g) for 3 h, cooled, and then heated at 2 °C/min between 50 and 280 °C. The data were corrected for ionic conduction above the glass transition of the dominant amorphous regions.

For amorphous samples, the permittivity was fit to the Havriliak−Negami relationship,[43] using all data points in the α-relaxation temperature range below the temperature of crystallization

$$\epsilon_r(T,\omega) - i\epsilon_i(T,\omega) = \epsilon_U(T) + (\epsilon_R(T) - \epsilon_U(T))\,(1 + [i\omega\tau_0(T)]^{\alpha})^{-\beta} \quad (2)$$

with ω the angular frequency, τ_0 the central dielectric relaxation time, α and β two phenomenological shape parameters, and ϵ_R and ϵ_U the relaxed ($\omega = 0$) and unrelaxed ($\omega = \infty$) values of ϵ_r, respectively. The temperature dependence of ϵ_U, α and β, was approximated by a linear relationship, that of $\epsilon_R - \epsilon_U$ by a T^{-1} relationship in accordance with theoretical predictions[44] (which are valid if the dipolar correlation factor does not vary much in the temperature range of the fit), and that of τ_0 by a Williams−Landel−Ferry law.[45]

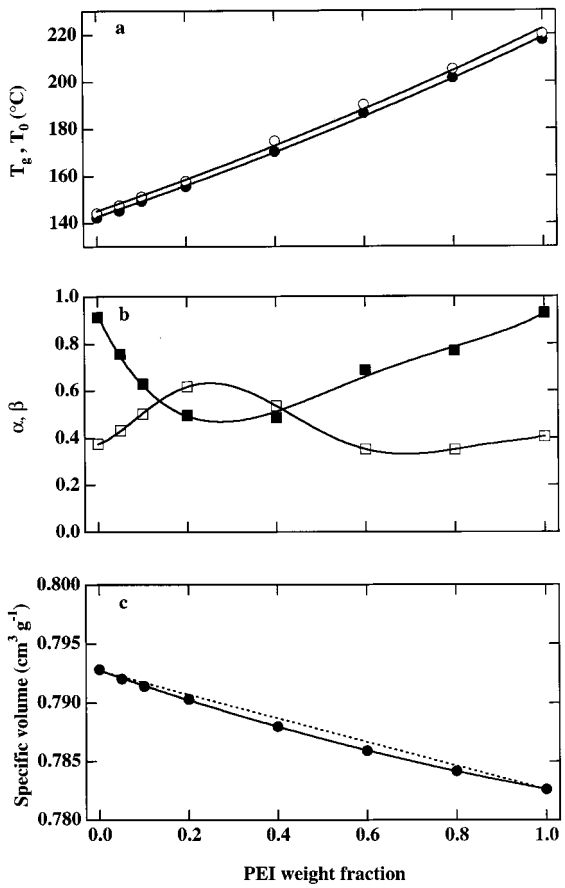

Figure 2. Evolution with PEI content of parameters characteristic of the starting amorphous PEEK/PEI blends. (a) Glass transition temperature by DSC (●) and dielectric T_0 (○), where T_0 is the temperature at which the central relaxation time (τ_0) equals 1 s (eq 2). The lines are fits to the Fox equation. (b) Havriliak−Negami shape parameters at T_0 (eq 2), denoted by ■ for α and by □ for β. (c) Specific volume. The dashed line represents a simple linear rule of mixture.

Density. Measurements were performed with a density gradient column (water/NaBr). Three measurements were performed for each sample.

Differential Scanning Calorimetry (DSC). Measurements were performed at 10 °C/min in a "Thermal Analysis" calorimeter calibrated with indium and zinc.

Results

Quenched Amorphous Samples. We checked the miscibility of PEEK and PEI in amorphous samples by dielectric spectroscopy, densitometry and DSC. As reported by others,[12,19−23] the blends exhibit a single glass transition by DSC (Figure 2a). Dielectric data in the α-relaxation range are well represented by Havriliak−Negami relationships,[43] provided the temperature dependence of the limiting dielectric constants and of the central relaxation time are taken into account (see Experimental Section). This analysis reveals a slight broadening of the relaxation curves, culminating for 30% added PEI, probably due to concentration fluctuations of small amplitude as reported by others for similar systems[46] (Figure 2b). The evolution of specific volume with blend composition departs slightly from linearity as noticed by others[23] (Figure 2c). This departure from a simple rule of mixture results either from a favorable energetic interaction between PEEK and PEI segments or from an improved spatial arrangement of PEEK and PEI chains in the blends, which

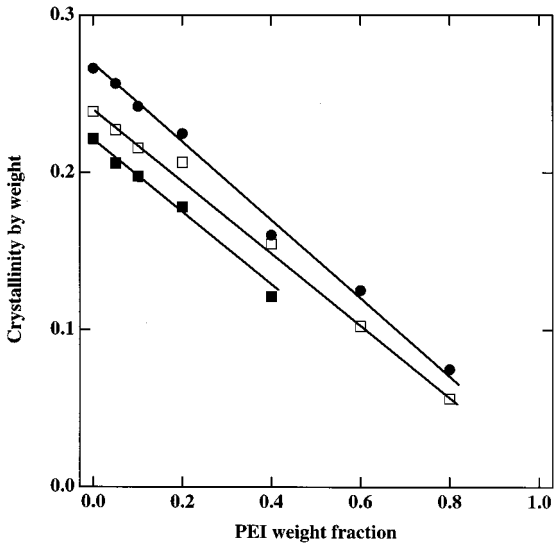

Figure 3. Evolution with PEI content of the crystallinity by weight for blends annealed for 9.5 h at $T_c = 280$ (●), 240 (□), and 200 °C (■).

reduces the free volume of the blend as compared to the separate homopolymers. In all cases, this leads to a slightly negative interaction parameter between PEEK and PEI. However, no attempt to quantify the interaction parameter was performed in the present study: the melting−recrystallization process occurring upon heating cold-crystallized PEEK[2] prevents us from performing a reliable Nishi−Wang[47] type of analysis.[48]

Annealed Samples. Crystallinity. The WAXS-determined crystallinity of the samples decreases linearly with PEI content for all annealing temperatures (Figure 3). The crystalline density and paracrystalline disorder were found to be strongly dependent on temperature, as is well-known for pure PEEK,[2,39] and were only marginally affected by PEI presence. PEI thus mainly acts as a diluent with respect to PEEK crystallinity and crystal quality.

Morphology. The morphology of thin solution-cast and annealed films was first examined by polarized optical microscopy. Spherulites became larger and less compact with increasing amounts of PEI, and finally, above 40% ($T_c = 280$ °C) or 60% PEI ($T_c = 240$ °C), they were found to be separated by large uncrystallized regions, suggesting interspherulitic segregation. These observations are similar to those reported by Hudson et al. on thin solution-cast films.[20]

Figure 4 presents TEM pictures of stained thin sections cut from bulk samples containing 60% and 80% of PEI annealed at 280 °C. PEEK-rich regions appear darker in these images.[42] For blends containing 60% of PEI (Figure 4a), no interspherulitic uncrystallized regions can be observed. White zones in the spherulites indicate copious interfibrillar segregation of PEI: spherulites appear relatively open. When PEEK content is decreased further to 20%, the spherulites become extremely open (Figure 4b). For these 20/80 PEEK/PEI blends, the openness and fineness of the spherulites allows to examine by TEM the spherulitic features down to the lamellar scale, especially at the outer boundary of spherulites.[42] Figure 4c and Figure 5 present large magnifications of lamellar stacks and isolated lamellae found in the 20/80 PEEK/PEI blend annealed at 280 °C. It is evident from these images that most lamellae tend to be grouped in stacks. However, at the spherulitic

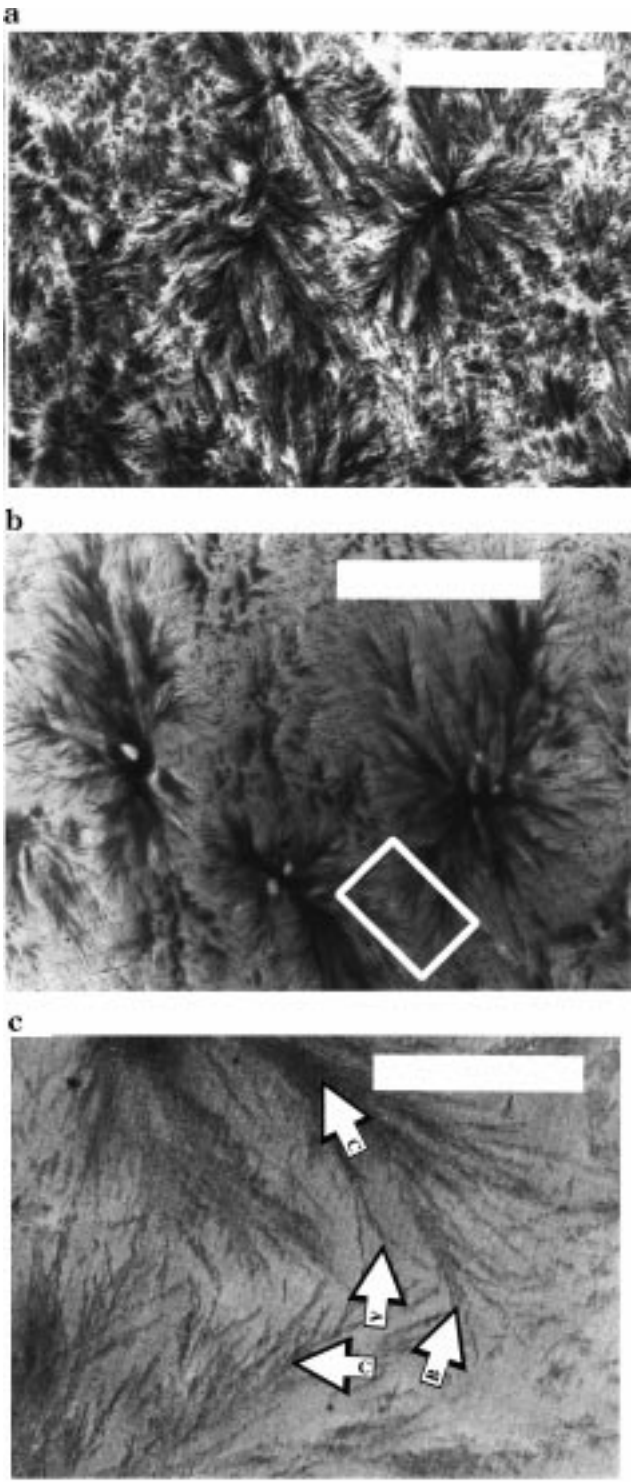

Figure 4. TEM micrographs of stained microtomes of cold-crystallized PEI-rich PEEK/PEI blends. PEEK appears black in these pictures. Key: (a) 40/60 PEEK/PEI blend isothermally crystallized for 9.5 h at 280 °C, scale bar 3.0 μm, (b) 20/80 PEEK/PEI blend isothermally crystallized for 9.5 h at 280 °C, scale bar 5.0 μm; (c) larger scale magnification of the rectangular area indicated in Figure 4b, scale bar 1.0 μm. Arrows indicate (A) an isolated lamella at the spherulitic periphery, (B) a short stack of parallel lamellae separated by PEI-rich zones at the spherulitic periphery, and (C) stacks of closely packed lamellae as found profusely inside spherulites and occasionally at their periphery. The absence of significant amounts of interlamellar PEI in these stacks results in them appearing as large black regions in the stained blends.

boundaries, it is not a rare event to detect isolated lamellae (arrows A and B in Figure 4c). Large PEI

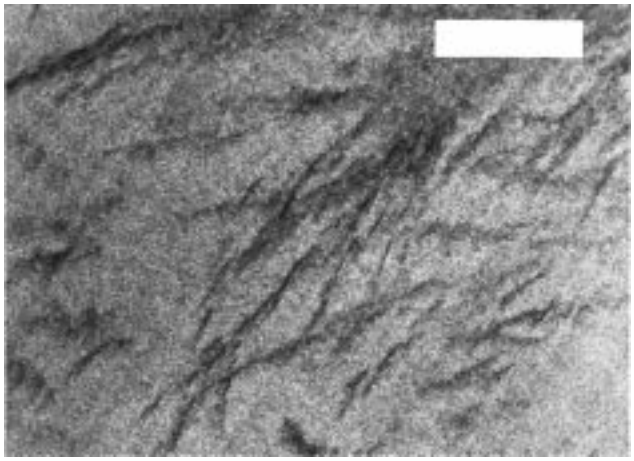

Figure 5. TEM micrograph (very large magnification) of a stained microtome of 20/80 PEEK/PEI blend cold-crystallized for 9.5 h at 280 °C. PEEK appears black in these pictures. Scale bar: 0.25 μm.

regions separate the spherulite fibrils (lamellar stacks); however, spherulites are almost adjacent and interspherulitic segregation is minor (Figure 4b). This is quite different from what we concluded from the examination of solution-cast films by optical microscopy (see ref 20 and above), most probably due to differences in nucleation density and chain mobility, reduced dimensionality, or even possible orientation effects induced by the substrates in thin films. Anyway, this indicates that one should be very prudent when trying to extrapolate morphologies observed on thin solution-cast films to bulk samples.

TEM observations on stained microtomes from blends richer in PEEK (at least 60% of PEEK) showed only rather dark and vague images.[42] Spherulites could still be clearly detected; however, the internal features of the spherulites could not be well resolved. No interspherulitic segregation occurs for such PEEK-rich blends upon annealing at 240 or 280 °C. For samples annealed at 200 °C, the situation is more difficult to analyze, because the annealing temperature is below the glass transition temperature of PEI. Consequently, kinetic effects (mobility) strongly interfere with crystallization, preventing in some instances full crystallization to occur.[49] The absence of white regions in stained microtomes of blends containing at least 60% of PEEK indicates that no large region consisting of pure PEI exists in these samples. However, very small regions strongly enriched in PEI could be detected in the 60/40 PEEK/PEI blend by another method. Unstained microtomes were exposed for a short time to methylene chloride, a good solvent for PEI. Upon observation by TEM, numerous pinholes were detected in the microtome, due to the dissolution of PEI in PEI-rich regions (Figure 6a). The same treatment was applied to other samples annealed at 280 °C: blends richer in PEEK were not affected by exposure to CH_2Cl_2, while the 20/80 PEEK/PEI blend fell into dust, in agreement with the existence of small amounts of interspherulitic PEI in this sample. The 40/60 PEEK/PEI blend after exposure to CH_2Cl_2 is shown in Figure 6b. Large gaps are observed in the microtome, corresponding to the white interfibrillar regions detected on the stained microtomes (Figure 4a).

From our TEM pictures, it is seen that interfibrillar PEI segregation is dominant even in the blends of small PEI contents. At the very periphery, the spherulites

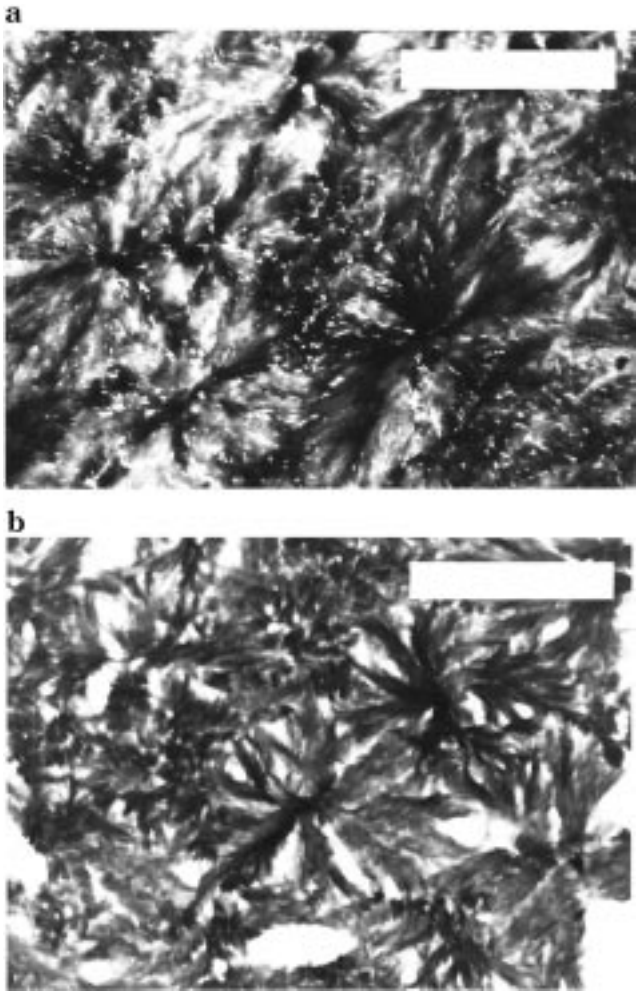

Figure 6. TEM micrographs of unstained microtomes after exposure to CH_2Cl_2. Pinholes in the films are due to the dissolution of PEI by CH_2Cl_2, and thus appear white in the pictures. Key: (a) 60/40 PEEK/PEI blend annealed for 9.5 h at 280 °C, scale bar 3.0 μm; (b) 40/60 PEEK/PEI blend annealed for 9.5 h at 280 °C, scale bar 3.0 μm.

are so finely open that isolated lamellae (arrow A in Figure 4c), or parallel lamellae separated by a whiter PEI-rich zone (arrow B in Figure 4c), are sometimes apparent. In these conditions, "interlamellar" inclusion of PEI thus occurs, albeit in a rather restricted amount. However, most lamellae tend to lie in relatively closed stacks (arrows C in Figure 4c), consistent with the previous findings of Lovinger et al.[50] for thin films of pure PEEK.

Small-Angle X-ray Scattering. Since TEM does not allow to decide on the characteristics of segregation for PEEK-rich blends, we have measured the SAXS for our samples. The parasitic-corrected data are shown in Figure 7, in bilogarithmic form. The amorphous samples (Figure 7a) exhibit a strong central scattering, which can be described in our experimental range by a s^{α} power law with an exponent $\alpha = -3.0 \pm 0.2$ (over 2−3 decades of intensity). The background due to thermal density fluctuations dominates the signal from $s = 0.01$ Å^{-1}. The existence of a strong central scattering in amorphous polymers is well-known and is usually ascribed to impurities or other macroscopic inhomogeneities. More surprising is the value for the exponent of the power law, since the apparent value of α is expected to be -4 or lower for nonfractal scatterers, while $\alpha = -3$ is not possible theoretically for fractal

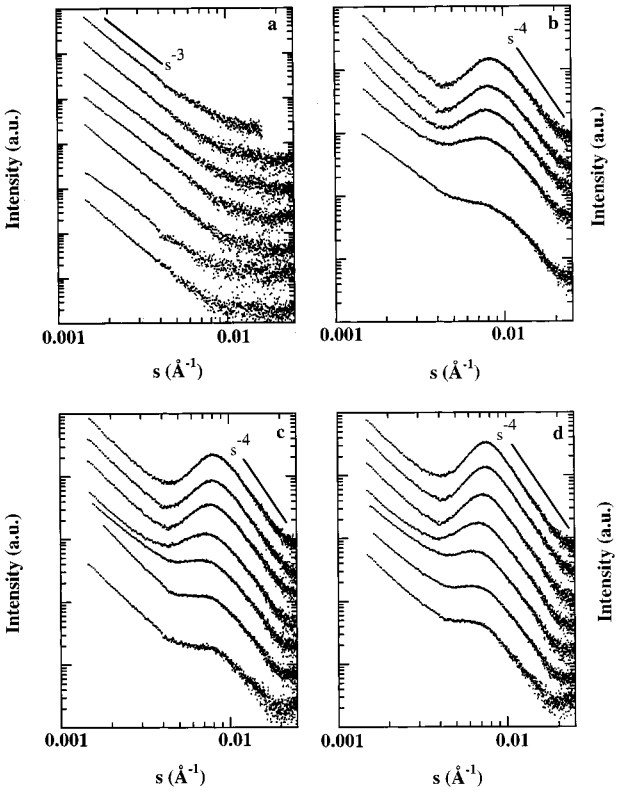

Figure 7. Small-angle X-ray scattering patterns of PEEK/PEI blends. Key: (a) amorphous samples (PEI fraction, from top to bottom: 0, 0.1, 0.2, 0.4, 0.6, 0.8, 1); (b) samples annealed at 200 °C for 9.5 h (PEI fraction, from top to bottom: 0, 0.05, 0.1, 0.2, 0.4); (c) samples annealed at 240 °C for 9.5 h (PEI fraction, from top to bottom: 0, 0.05, 0.1, 0.2, 0.4, 0.6, 0.8); (d) samples annealed at 280 °C for 9.5 h. (PEI fraction, from top to bottom: 0, 0.05, 0.1, 0.2, 0.4, 0.6, 0.8). The traces have been displaced vertically for clarity.

scatterers.[51] This point is, however, outside the scope of the present paper.

Upon annealing, a broad reflection peak appears in the SAXS plots (Figure 7b−d). The results at very low angles are still dominated by a power law with an exponent near −3, which is clearly reminiscent of the scattering from the pure amorphous samples. At large angles, the scattering is again well-described by a s^{β} power law, with β close to −4 in accordance with Porod's law for smooth scatterers.[52] Between these two regions, the scattering reflects the interferences between the X-ray wave scattered at the interfaces of the lamellar structures. For the largest angles, the scattering is dominated by the signal arising from thermal density fluctuations (TDF) in the amorphous regions.

To allow for an easier comparison of the broad reflection peaks for the different samples, we have subtracted the TDF scattering from the SAXS (approximated by a constant), subtracted the s^{-3} power law dominating the scattering at very low angles, and normalized the SAXS by the PEEK content. The results of this treatment are displayed in Figure 8a for the samples annealed at 280 °C (other annealing temperatures give similar curves and are not reproduced here). The normalized SAXS fall on a single master curve between $s = 0.009$ and 0.02 Å^{-1} (Porod's range), from which two pieces of information can be obtained. First, density transition layers at the surface of the lamellae are identical for all samples, independent of PEI content. Second, the crystal (lamellar) thickness is rather

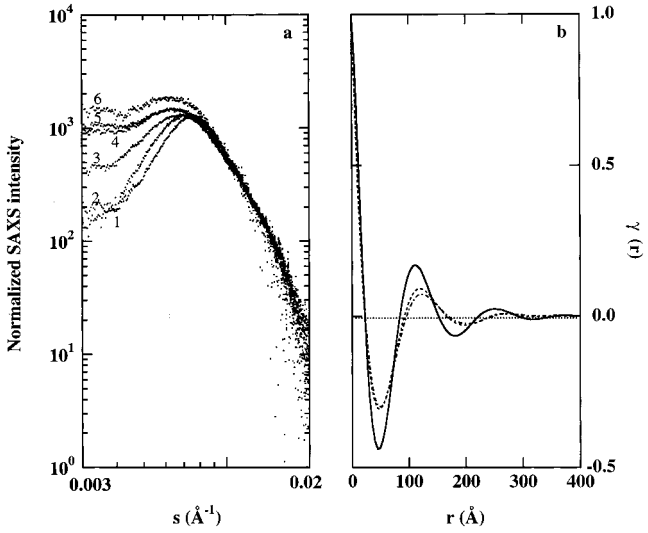

Figure 8. (a) Corrected SAXS patterns for PEEK/PEI blends annealed at 280 °C for 9.5 h. The curves have been normalized by PEEK content (curve number/PEI fraction: 1/0; 2/0.1; 3/0.2; 4/0.4; 5/0.6; 6/0.8). (b) Typical one-dimensional correlation functions computed from the SAXS intensity, shown for samples annealed for 9.5 h. at 280 °C. Continuous line: pure PEEK; dashed line: PEEK/PEI 80/20; dashed−dotted line: PEEK/PEI 60/40).

constant from sample to sample. Indeed, the scattered intensity in Porod's range is proportional to the total surface of interfaces (S) in the illuminated sample;[52] other proportionality factors are constant, neglecting the extremely small difference of electron density between pure PEI and amorphous PEEK. The existence of a master curve after normalization by PEEK content thus indicates that S is proportional to PEEK content (ϕ_{PEEK})

$$S = K\phi_{PEEK} \tag{3}$$

where K is a constant. Moreover, the volume crystallinity can be written as

$$\phi_c = SL_c/2V = (K/2V)\phi_{PEEK}L_c \tag{4}$$

with V the illuminated sample volume and L_c the average lamellar thickness. Since crystallinity is experimentally found to be proportional to ϕ_{PEEK} (Figure 3), it follows that L_c must be rather constant whatever the PEI content (here we have neglected the very small differences between crystallinity by weight and by volume). Thus, from these very general observations, we may safely conclude that the lamellar crystals are similar in thickness within experimental precision for all the blends annealed at a given temperature. The only requirement for this conclusion to be valid is that the scatterers be of lamellar nature, which is clearly confirmed by TEM. In particular, this conclusion is valid whatever the details of the spatial distribution of lamellae.

Furthermore, significant differences among the normalized scattering data for the blends are observed between $s = 0.003$ and 0.007 Å^{-1}, i.e., on the low-angle side of the broad reflection. It is important to note that these differences can already be observed on the uncorrected data (Figure 7d), which indicates that they do not result from the corrections applied to the data. As PEI content is increased in the blends, the scattering increases in this s range, with a parallel shift of the reflection maximum to lower angles. Since crystals

have been demonstrated to be constant in thickness, the excess scattering at low angles must be related to the development of regions of increasing size separating crystalline lamellae, as the PEI content increases.

To go a step further, we have computed the one-dimensional correlation functions from the SAXS data, i.e., the normalized Fourier transform of the Lorentz-corrected scattered intensity: s^2 was used as Lorentz factor, since the systems are clearly lamellar (TEM) and isotropic (see Experimental Section). Extrapolation to large angles was performed using scaling laws, but their effect was found to be of minor importance to the resulting correlation functions. The correlation functions ($\gamma(r)$) were analyzed in a conventional way,[53,54] using the following relationships:

$$\phi_{c,lin}(1 - \phi_{c,lin})L = r_0 \quad (5)$$

$$L_a = (1 - \phi_{c,lin})L \quad (6)$$

$$L_c = \phi_{c,lin}L \quad (7)$$

Here L is the long spacing determined from the first subsidiary maximum of the correlation function, and r_0 is the first intercept of the correlation function with the line $\gamma(r) = 0$. L_a denotes the average thickness of the interlamellar amorphous regions, L_c denotes the average crystal thickness, and $\phi_{c,lin}$ is the linear crystallinity, i.e., the ratio L_c/L. Equation 5 provides two possible values for $\phi_{c,lin}$, whose sum equals 1, in accordance with Babinet's reciprocity theorem. We have selected the smaller of these values as $\phi_{c,lin}$, following the homogeneous model for the lamellar structure of pure PEEK; the reverse selection would correspond to the heterogeneous model. The linear crystallinity of pure PEEK samples was thus found to be 0.27 ± 0.01, in reasonable agreement with the WAXS-determined crystallinity (Figure 3), consistent with the homogeneous model of PEEK microstructure.

For the annealing temperature of 200 °C, no dependence of the long period with PEI content was detected. These data are not discussed further in this paper, as they may be strongly dependent on kinetic effects, due to the close proximity of the annealing temperature with the glass transition of pure PEI.[49] The evolution of the SAXS-derived structural parameters with PEI content is reported in Figure 9, for annealing temperatures of 240 and 280 °C. The correlation functions for the 80% PEI samples could not be computed, because the small amount of the SAXS intensity originating from the semicrystalline lamellar stacks, as compared to other sources of scattering, did not allow us to perform a reliable computation of $\gamma(r)$ for these samples. The average distance between the centers of neighboring lamellae (i.e., the long period, L) first increases with PEI addition, but beyond 20% added PEI, it remains constant. The lamellar thickness L_c is independent of PEI content, in agreement with our conclusion discussed in the previous section. The thickness of the interlamellar amorphous region behaves similarly to the long period, first increasing with PEI addition and then saturating beyond 20% added PEI. The limited extent of the variations of L and L_a requires one to exercise caution when discussing the SAXS results. In this respect, it should first be noted that we have previously reported qualitatively similar results,[26] with the long period taken as the distance corresponding to the maximum of the Lorentz-corrected SAXS intensity, and with L_a and L_c computed from fits of the general paracrystalline model[55] to the SAXS data. Second, it is interesting to remark that a small increase of long period with PEI addition was also detected by others,[12] although not considered to be significant at that time. The reproductibility of these results in the present work indicates that this variation may be considered to be real, despite being of limited extent. This conclusion is also supported by the dielectric results to be presented shortly.

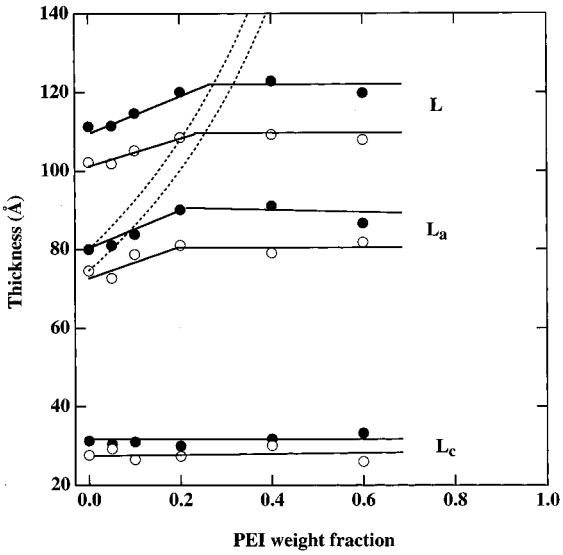

Figure 9. Evolution of the long period (L), the average thickness of the interlamellar regions (L_a), and the average thickness of the crystalline lamellae (L_c) with PEI content. Dashed lines present the evolution of L_a expected for complete interlamellar PEI segregation. (●, blends annealed at 280 °C for 9.5 h; ○, blends annealed at 240 °C for 9.5 h).

The increase of L_a with PEI addition suggests partial interlamellar PEI inclusion. The extent of interlamellar inclusion is, however, quite small. Below 20% added PEI, the increase of L_a with PEI is only 30% of the expected value for full interlamellar inclusion; for larger PEI contents, this proportion decreases dramatically, as indicated by the departures from the calculated values for complete interlamellar inclusion (dashed lines in Figure 9). Comparison of correlation functions reveals that not only does the addition of PEI shift the first correlation maximum but also the distribution of interlamellar distances becomes less symmetric, with a broadening toward larger distances (Figure 8b). This suggests that the remaining PEI may tend to accumulate in regions of larger size, which could be considered as precursors to interfibrillar spaces. The size of these regions must, however, be still quite restricted for samples containing less than 60% PEI, since TEM failed to disclose the presence of pure PEI regions in these samples.

Dielectric Spectroscopy. The evolution of the imaginary part of the dielectric permittivity with temperature is displayed in Figure 10a, for samples annealed at 280 °C (4 kHz). For these samples, no structural changes occur upon heating to 280 °C;[2] consequently, the features observed in Figure 10a are representative of the starting materials (this would not be the case for samples annealed at lower temperatures). Starting from pure PEEK, the addition of PEI first moves the α-relaxation to higher temperatures, while broadening the relaxation. Then, starting from

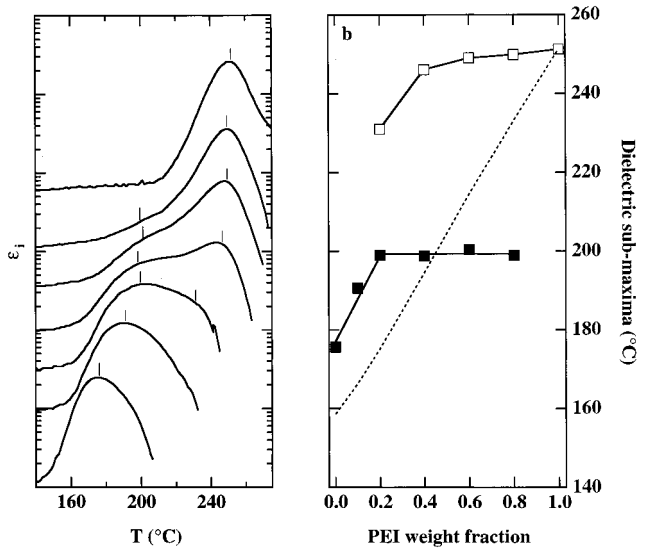

Figure 10. (a) Dielectric loss of PEEK/PEI blends annealed at 280 °C for 9.5 h vs temperature (test frequency: 4 kHz). The curves have been displaced vertically for clarity. PEI weight fraction, from bottom to top: 0, 0.1, 0.2, 0.4, 0.6, 0.8. The top curve corresponds to pure PEI (not annealed). (b) Evolution with PEI content of the temperature locations of the dielectric relaxation submaxima of PEEK/PEI blends annealed at 280 °C for 9.5 h (test frequency: 4 kHz). Key: (■) the lower temperature; (□) the upper temperature. The dashed line is the corresponding result for quenched amorphous samples under the same conditions.

20% added PEI, a second relaxation peak centered near 250 °C progressively develops, eventually becoming the main feature of the curve. To increase the accuracy in locating the dielectric submaxima, these were determined from the minima of the second derivative of the $\epsilon_i(T)$ curves. Such a procedure is often used by spectroscopists to artificially enhance resolution.[56] Results are presented in Figure 10b. The temperature location of the first relaxation increases with PEI content, then saturates at about 200 °C above 20% PEI. The second relaxation is difficult to separate below 40% PEI; its temperature location slightly increases with PEI content and saturates around 250 °C, the relaxation temperature of pure PEI. These results are similar to those reported recently by others,[25] and bear much resemblance with what was reported earlier for blends of poly(butylene terephthalate) and poly(arylate) (PBT/PAr).[57]

Discussion

Mode of Segregation and Attribution of the Relaxations. It is customary to distinguish in semicrystalline blends three amorphous regions: interlamellar regions, interfibrillar regions, and interspherulitic regions. However, as pointed out previously, the distinction between interlamellar and interfibrillar regions is lacking clarity for very open spherulites such as those obtained for the 20/80 PEEK/PEI blend: fibrils become thinner from the center to the periphery of the spherulite, eventually giving rise to isolated lamellae at the border of the spherulites. Moreover, for such open spherulites, the differences between interfibrillar and interspherulitic regions are minor. This is because the openness of the spherulites implies that interspherulitic regions are contiguous with interfibrillar regions; consequently, both regions will have similar compositions and relaxation spectra, except for the small portion of interfibrillar regions directly adjacent to PEEK crystals. This explains why no new relaxation appears on passing from the blend containing 60% PEI, with no interspherulitic segregation, to the blend containing 80% PEI, where a small amount of interspherulitic segregation occurs. Nevertheless, the distinction between interspherulitic and interfibrillar PEI is still of practical interest, because the macroscopic behavior of these samples can be quite different. For instance, upon immersion in methylene chloride, the 20/80 PEEK/PEI blend annealed at 280 °C fragments into dust, while the 40/60 PEEK/PEI blend preserves its integrity owing to the numerous interspherulitic contacts existing in this sample.

For blends containing less than 80% PEI, TEM shows the absence of interspherulitic segregation. SAXS also indicates that most PEI is excluded from interlamellar regions. Thus, at the end of the crystallization process, PEI is essentially located in interfibrillar regions, with a small fraction of PEI remaining in the interlamellar regions as suggested by SAXS. Interfibrillar regions do not contribute much to the SAXS signal, first because their sizes may be too large in comparison with the lowest s value of our experimental range and second because their electron density is only slightly different from the average electron density of the lamellar stacks (fibrils). Nevertheless, their presence is partly responsible for the excess scattering detected for the blends between $s = 0.003$ and 0.007 Å^{-1}, corresponding to distances of 150−350 Å.

We can thus sum up our observations in the following way. Below 20% added PEI, the addition of PEI results in a slight increase of L_a, due to limited interlamellar inclusion, and in the development of larger amorphous regions which are enriched in PEI and separate stacks of more closely grouped lamellae. These larger regions are nascent interfibrillar regions that are still restricted in their size; therefore, PEI is always mixed in these regions with amorphous PEEK segments attached to neighboring crystals, as revealed by the absence of relaxation due to pure PEI regions and also by the absence of white regions in stained TEM samples. In this range of PEI content, the first dielectric subrelaxation moves progressively to higher temperatures, consistent with the evolution of L_a. This relaxation originates essentially from interlamellar regions and nascent interfibrillar regions. However, the relaxation broadens significantly toward higher temperatures with PEI addition, indicating that interfibrillar regions of larger sizes and of richer PEI content progressively develop.

Above 20% added PEI, the amount of PEI included in the interlamellar regions saturates, as indicated by the location of the first dielectric relaxation subpeak and the value of L_a. The remaining added PEI then accumulates entirely in the interfibrillar regions, thereby increasing their average size and allowing regions of pure PEI to occur in the samples. These regions are clearly detected by the appearance of the second subrelaxation and by the TEM appearance of white regions in stained microtomed cuts or holes in unstained cuts washed by methylene chloride.

From this analysis, we conclude that the dielectric relaxation subpeak located at the higher temperature corresponds to the relaxation of regions containing almost pure PEI. It originates from portions of interfibrillar spaces sufficiently away from PEEK crystals, so that no PEEK amorphous segments attached to a

crystal (loose loops, dangling chains, ...) may be present. For the blend containing 80% PEI, this relaxation also originates from interspherulitic regions. In contrast, the first relaxation subpeak originates from noncrystalline regions located close to PEEK crystals. Interlamellar regions obviously make a significant contribution to this relaxation, but portions of interfibrillar spaces near crystal surfaces may also contribute to this relaxation. This explains why this relaxation is the only one to be detected when nascent interfibrillar spaces exist in the samples. This interpretation is compatible with the ideas proposed some time ago by ourselves[26] and, more recently, by Bristow and Kalika.[25]

Homogeneous vs Heterogeneous Models of PEEK Lamellar Microstructure. We return briefly to the problem of selecting one of the two solutions of eq 5 to $\phi_{c,lin}$, i.e., to the question of homogeneous vs heterogeneous models in describing the lamellar microstructure of pure PEEK. Our selection of the smallest value for $\phi_{c,lin}$ is logical, since it leads to constant crystal thickness and to an increase of the amorphous interlayer thickness with PEI addition, as expected for interlamellar inclusion. The reverse attribution would in our case lead to a constant thickness of the amorphous interlayer and to an increase of crystal thickness with PEI content. Such a picture would be difficult to reconcile, considering the high degree of supercooling of our samples (the thermodynamic melting temperature of PEEK is reported to be 395 °C[58] or 389 °C[5]) and the fact that PEEK/PEI blends exhibit small or negligible melting point depression.[12,19,59] Moreover, our selection is supported by dielectric results, which show an excellent correlation between the evolution with PEI content of the temperature location of the first glass subrelaxation, associated to interlamellar regions, and the evolution of the thickness of the amorphous interlayer (compare Figure 9 with Figure 10b). Furthermore, it becomes even more difficult to understand the appearance of nearly pure PEI regions in terms of the heterogeneous model, since PEI should remain miscible with noncrystalline PEEK in the proposed large amorphous gaps.

Finally, it is possible to obtain an estimation for the lamellar thickness from TEM images of the most dilute blends (Figure 5). Obviously, only lamellae having their normals lying in the plane of the images will be suited for such an estimation. These lamellae are also the most contrasted and appear as the thinnest. Moreover, since both amorphous and crystalline PEEK are readily stained by the staining agent,[42] only isolated PEEK lamellae surrounded by large amounts of PEI can be resolved in our TEM pictures. Such lamellae exclusively appear in PEI-rich blends.[42] We have scanned the TEM images of such dilute blends and established an average profile for the photographic optical density of such lamellae (Figure 11). This profile was obtained by averaging measurements performed on different lamellae, corresponding to a total length of about 200 nm. The profile can be represented by a Gaussian having 2.2 nm as standard deviation (full width at half-maximum, FWHM, of 5.0 nm). It is obvious that the FWHM of the Gaussian represents an upper bound for the lamellar thickness. Our estimation of lamellar thickness from the SAXS correlation function for the blends annealed at 280 °C amounts to about 3.0 nm, while heterogeneous models would correspond to lamellar thicknesses on the order of 8.5 nm, well above the upper bound provided by TEM. Since crystal thicknesses as obtained from SAXS correlation functions are probably slightly underestimated,[2] it is clear that our selection of the smaller value for $\phi_{c,lin}$ in eq 5 is more consistent with our results obtained in direct space and relaxation space.

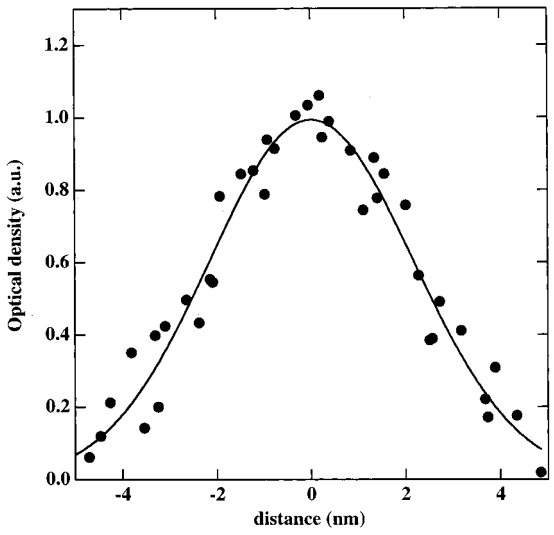

Figure 11. Average profile for the TEM photographical optical density of the best-contrasted lamellae obtained on stained microtomes of the blend PEEK/PEI 20/80 annealed for 9.5 h. at 280 °C. The continuous line is a Gaussian fit to the data (standard deviation: 2.2 nm).

One could object that the isolated lamellae observed by TEM are not representative of the lamellae grouped into stacks that are responsible for the SAXS signal. However, a qualitative examination of TEM micrographs of Lovinger et al.[20] on PEEK/PEI thin films, where stacks of lamellae can be seen with emerging isolated lamellae at their tips, does not indicate any significant difference between isolated lamellae at the tips of stacks and lamellae further inside the stacks. Hence, we may safely conclude that our comparison between TEM and SAXS is warranted. The reasonable agreement found between TEM and SAXS validates the homogeneous model for the lamellar microstructure of *pure* PEEK cold-crystallized below 300 °C and invalidates the heterogeneous models discussed in the literature[3,12,13] for *pure* PEEK. For PEEK/PEI blends, the presence of interfibrillar PEI-rich regions evidently results in a heterogeneous microstructure; however, the volume fraction of interfibrillar spaces tends to zero with decreasing PEI dilution.

Given such low values of lamellar thickness, one would expect a substantial reduction of the melting temperature (T_m) of the samples as compared to the melting temperature of the hypothetical extended chain infinite crystal ($T_m°$). We have computed T_m for 30 Å-thick crystals by the Gibbs−Thomson equation, using thermodynamic parameters (melting enthalpy, planar surface energy of lamellae, and $T_m°$) published in the literature.[6,58] The computed melting temperatures are located between 275 and 310 °C, depending on the selected thermodynamic parameters. These values compare well with the temperature locations of the first melting endotherm of PEEK and PEEK/PEI samples (290−300 °C), consistent again with the homogeneous model of PEEK microstructure.

Structure of Interlamellar Regions: Interlamellar vs Interfibrillar Segregation. Interspherulitic segregation is usually interpreted as arising from a

large diffusion coefficient for the noncrystallizable diluent combined with a comparatively slow radial growth rate of the spherulite. Keith and Padden[18] have translated this notion into a semiquantitative model, in which a central role is played by the parameter $\delta = D_c/G$, with D_c the mutual diffusion coefficient of the diluent in the melt and G the radial growth rate of the spherulite. It has been sometimes considered that δ defines the scale of segregation, interlamellar segregation occurring for δ's on the order of the average interlamellar distance and interspherulitic segregation for δ's on the order of a spherulite radius, for example.[12] In this regard, it should be noted that the original work of Keith and Padden[18] actually concentrated on large-scale spherulitic features detected by optical microscopy, which limits the relevance of δ to the supralamellar scale as acknowledged by Keith and Padden themselves. The inadequacy of relating δ to lamellar-scale features was clearly stated again years later by Bassett[60] in a review of his TEM works on polymer microstructure. Therefore, although δ may be relevant to predict interfibrillar vs interspherulitic segregation, its use to predict interlamellar segregation is much less warranted.

In the case of pure PEEK, TEM photographs of Lovinger et al.[50] indicate a clear trend of lamellae to grow more or less closely together, instead of randomly over space. Therefore, in the case of PEEK/PEI blends, the disfavored interlamellar inclusion of PEI is most likely due to this tendency of lamellae to prefer a close parallel growth. Such a tendency is by no means limited to PEEK; similar observations have been made for other polymers as well.[60,61] The origin of this trend most probably lies in the structure of the noncrystalline regions at the vicinity of a crystal surface, which favors the growth of a close parallel lamella. In this regard, it is probably significant that all aromatic semicrystalline polymers studied to date tolerate only a limited amount of interlamellar segregation (PBT in PBT/PAr blends,[57] PEEK in PEEK/PEI blends, and poly(ethylene terephthalate) in PET/PEI blends[62]), while full interlamellar segregation is a frequent occurrence for semicrystalline blends made of more flexible polymers (see Table 1 in ref 63 for a review). This specific behavior is thus probably related to the increased stiffness of aromatic chains. Although the role of kinetic factors (aromatic polymers usually are slow crystallizers) cannot be fully ruled out, the fact that PEI inclusion reaches a plateau with increasing bulk PEI content indicates that kinetic considerations are not the major factor. That is, the discontinuous character of PEI inclusion is difficult to reconcile with kinetic parameters such as crystal growth rate and PEI diffusion, which are continuously varying functions of bulk PEI content.

These observations suggest that the nature of noncrystalline segments in interlamellar regions of semicrystalline PEEK is quite different from that of the fully disordered bulk amorphous PEEK. In some way, it may be more akin to a relatively disordered liquid crystalline phase. In this context, it is of interest to note the similarity in mixing behavior between PEI in PEEK interlamellar regions on one hand, to the flexible polymer components in liquid crystals on the other hand. For example, both theory[64] and experiments[65] show a nearly complete exclusion of random-coiled flexible polymers in the nematic solution of rodlike polymers, despite very favorable mixing exchange energies. In this regard, the general problem of the structure of noncrystalline regions in the vicinity of lamellar crystals, the dissipation of crystalline order in particular, offers challenging opportunities for further research.

Conclusion

A consistent picture for the morphology of PEEK/PEI blends has been obtained by combining the results of investigations by WAXS, SAXS, dielectric spectroscopy, and TEM experiments. Below 20% added PEI, the addition of PEI results in an increase of the thickness of the interlamellar amorphous regions (L_a), due to partial PEI interlamellar segregation, and in the development of nascent interfibrillar regions. In this range of PEI content, the dielectric α-relaxation moves progressively to higher temperatures, consistent with the evolution of L_a. This relaxation originates from regions adjacent to PEEK crystals, mainly interlamellar regions but also portions of interfibrillar spaces at crystal surfaces. The relaxation broadens significantly toward higher temperatures with PEI addition, indicating that PEI-enriched interfibrillar regions of larger size progressively develop.

Above 20% added PEI, the amount of PEI included in the interlamellar regions saturates. Simultaneously, the α-relaxation peak splits in two subpeaks. The first subpeak still mostly corresponds to the relaxation of interlamellar regions (the evolution of its temperature location follows closely the behavior of L_a). The second subpeak develops progressively at higher temperature, corresponding to the relaxation of nearly pure PEI regions created by the accumulation of this polymer in interfibrillar regions. For the 20/80 PEEK/PEI blend, interspherulitic regions of pure PEI also occur. TEM observations on stained thin sections from bulk samples confirm these conclusions.

We have also pointed out that the restricted character of the PEI interlamellar inclusion indicates a clear preference of lamellae to grow tightly packed together. We have suggested that this result is related to the structure of the noncrystalline regions near crystal surfaces and that the reduced flexibility of the chains could be a factor promoting this behavior in aromatic semicrystalline polymers.

Finally, we have presented related experimental evidences which clearly demonstrate the validity of homogeneous models in representing the lamellar microstructure of pure PEEK crystallized below 300 °C. Such PEEK samples comprise thin lamellar crystals separated by a thicker amorphous interlayer, grouped into stacks of limited coherence and homogeneously filling all the sample volume. This validates our previous interpretation of the SAXS results for PEEK samples subjected to various thermal treatments.[2] It also confirms the previous finding that the variation of the glass transition temperature of semicrystalline PEEK is correlated to the thickness of amorphous interlayers.[14]

Acknowledgment. The authors are indebted to Prof. T. P. Russell for his help in performing the SAXS experiments, to Dr. G. L. Gorman for obtaining the WAXS spectra of the samples, to Mrs. H. Truong for performing some DSC experiments, and to Mrs. P. Lipnik for her help with TEM experiments. We are pleased to acknowledge Dr. C. Bailly at GE Plastics (Bergen-op-Zoom, The Netherlands) for providing Ultem 1000 PEI resin, and Dr. P. T. McGrail at ICI (Wilton,

U.K.) for supplying the Victrex 150P PEEK powder. This work benefited from the financial support of IBM Belgium and of the Belgian National Fund for Scientific Research. A.M.J. further expresses his gratitude to NATO for a research fellowship and to the U.S. Government for the award of a Fulbright-Hays research scholar grant-in-aid in 1993. This work was performed in part at the Stanford Synchrotron Radiation Laboratory which is partially supported by the U.S. Department of Energy, Office of Basic Energy Sciences.

References and Notes

(1) PEEK stands for poly(oxy-1,4-phenyleneoxy-1,4-phenylenecarbonyl-1,4-phenylene); PEI stands for poly([2,2′-bis(3,4-dicarboxyphenoxy) phenylpropane]-2-phenylene-bisimide).
(2) Jonas, A. M.; Russell, T. P.; Yoon, D. Y. *Macromolecules* **1995**, *28*, 8491.
(3) Verma, R. K.; Hsiao, B. S. *Trends Polym. Sci.* **1996**, *4*, 312.
(4) Blundell, D. J. *Polymer* **1987**, *28*, 2248.
(5) Lee, Y.; Porter, R. S. *Macromolecules* **1987**, *20*, 1336.
(6) Lee, Y.; Porter, R. S.; Lin, S. J. *Macromolecules* **1989**, *22*, 1756.
(7) Bassett, D. C.; Olley, R. H.; Al Raheil, I. A. M. *Polymer* **1988**, *29*, 1745.
(8) Cheng, S. Z. D.; Cao, M.-Y.; Wunderlich, B. *Macromolecules* **1986**, *19*, 1868.
(9) Cebe, P.; Hong, S. D. *Polymer* **1986**, *27*, 1183.
(10) Krüger, K.-N.; Zachmann, H. G. *Macromolecules* **1993**, *26*, 5202.
(11) Verma, R. K.; Velikov, V.; Kander, R. G.; Marand, H.; Chu, B.; Hsiao, B. *Polymer* **1996**, *37*, 5357.
(12) Hsiao B. S.; Sauer, B. B. *J. Polym. Sci.: Polym. Phys.* **1993**, *31*, 901.
(13) Verma, R.; Marand, H.; Hsiao, B. *Macromolecules* **1996**, *29*, 7767.
(14) Jonas, A.; Legras, R. *Macromolecules* **1993**, *26*, 813.
(15) Fougnies, C.; Damman, P.; Villers, D.; Dosière, M.; Koch, M. H. J. *Macromolecules* **1997**, *30*, 1385.
(16) Fougnies, C.; Damman, P.; Dosière, M.; Koch, M. H. J. *Macromolecules* **1997**, *30*, 1392.
(17) Defieuw, G.; Groeninckx, G.; Reynaers, H. *Polymer* **1989**, *30*, 2164.
(18) Keith, H. D.; Padden, F. J. *J. Appl. Phys.* **1964**, *35*, 1270; *Ibid*. **1964**, *35*, 1286; *Ibid*. **1963**, *34*, 2409.
(19) Crevecoeur, G.; Groeninckx, G. *Macromolecules* **1991**, *24*, 1190.
(20) Hudson S. D.; Davis D. D.; Lovinger, A. J. *Macromolecules* **1992**, *25*, 1759.
(21) Harris, J. E.; Robeson, L. M. *J. Appl. Polym. Sci.* **1988**, *35*, 1877.
(22) Goodwin, A. A.; Hay, J. N.; Mouledous, G. A. C.; Biddlestone, F. In *Integration of Fundamental Polymer Science and Technology*; Lemstra, P. J., Kleintjens, L. A., Eds.; Elsevier: London, 1990; Vol. 5, p 44.
(23) Chen, H.-L.; Porter, R. S. *Polym. Eng. Sci.* **1992**, *32*, 1870.
(24) Lee, C. H.; Okasa, T.; Saito, H.; Inoue, T. *Polymer* **1997**, *38*, 31.
(25) Bristow, J. F.; Kalika, D. S. *Polymer* **1997**, *38*, 287.
(26) Jonas, A. M.; Russell, T. P.; Yoon, D. Y. *Proc. Am. Chem. Soc. Div. Polym. Mater. Sci. Eng.* **1994**, *70*, 394.
(27) Russell, T. P.; Ito, H.; Wignall, G. D. *Macromolecules* **1988**, *21*, 1703.
(28) Hahn, B.; Wendorff, J.; Yoon, D. Y. *Macromolecules* **1985**, *18*, 718. Yoon, D. Y.; Ando, Y.; Rojstaczer, S.; Kumar, S. K.; Alfonso, G. C. *Makromol. Chem. Macromol. Symp.* **1991**, *50*, 183.
(29) Kumar, S. K.; Yoon, D. Y. *Macromolecules* **1989**, *22*, 4098.
(30) Kumar, S. K.; Yoon, D. Y. *Macromolecules* **1991**, *24*, 5414.
(31) Mandelkern, L. *Chemtracts—Macromol. Chem.* **1992**, *3*, 347.
(32) Jonas, A.; Legras, R. *Polymer* **1991**, *32*, 2691.
(33) Daoust, D.; Devaux, J.; Godard, P.; Jonas, A.; Legras, R. In *Advanced Thermoplastic Composites*; Kausch, H. H., Ed.; Carl Hanser Verlag: Munich, Germany, 1992; p 3.
(34) Hourdet, D.; Muller, G.; Vincent, J. C.; Avrillon, R.; Robert, E. In *Polyimides and other High-Temperature Polymers*; Abadie, M. J. M., Sillion, B., Eds.; Elsevier: Amsterdam, 1991; p 507.
(35) Klug, H. P.; Alexander, L. E. *X-ray Diffraction Procedures in Polycrystalline and Amorphous Materials*, 2nd ed.; J. Wiley & Sons: New York, 1974.
(36) Ruland, W. *Acta Crystallogr.* **1961**, *14*, 1180. Ruland, W. *Polymer* **1964**, *5*, 89.
(37) Vonk, C. G. *J. Appl. Crystallogr.* **1973**, *6*, 148.
(38) Veeraraghavan, V. G.; Rubin, H.; Winchell, P. G. *J. Appl. Crystallogr.* **1977**, *10*, 66.
(39) Wakelyn, N. T. *J. Polym. Sci. C: Polym. Lett.* **1987**, *25*, 25. Hay, J. N.; Langford, J. I.; Lloyd, J. R. *Polymer* **1989**, *30*, 489. Deslandes, Y.; Alva Rosa, E. *Polym. Commun.* **1990**, *31*, 269.
(40) Hosemann, R. *J. Appl. Phys.* **1963**, *34*, 25.
(41) Russell, T. P. in *Handbook on Synchrotron Radiation*; Brown, G., Moncton, D. E., Eds.; Elsevier Science Publishers: Amsterdam, 1991; p 379.
(42) Ivanov, D. A.; Lipnik, P. D. M.; Jonas, A. M. *J. Polym. Sci.: Polym. Phys.* **1997**, *35*, 2565.
(43) Havriliak, S.; Negami, S. *Polymer* **1967**, *8*, 161.
(44) Fröhlich, H. *Theory of Dielectrics, Dielectric Constant and Dielectric Losses*; Oxford University Press: Oxford, England, 1949.
(45) Williams, M. L.; Landel, R. F.; Ferry, J. D. *J. Am. Chem. Soc.* **1955**, *77*, 3701.
(46) Katana, G.; Fischer, E. W.; Hack, Th.; Abetz, V.; Kremer, F. *Macromolecules* **1995**, *28*, 2714.
(47) Nishi, T.; Wang, T. T. *Macromolecules* **1975**, *8*, 909.
(48) Runt, J.; Gallagher, K. P. *Polym. Commun.* **1991**, *32*, 180.
(49) Ivanov, D. A.; Jonas, A. M. *J. Polym. Sci.: Polym. Phys. Ed.* **1998**, *36*, 919.
(50) Lovinger, A. J.; Hudson, S. D.; Davis, D. D. *Macromolecules* **1992**, *25*, 1752.
(51) Schmidt, P. W. *J. Appl. Crystallogr.* **1991**, *24*, 414.
(52) Porod, G. In *Small Angle X-ray Scattering*; Glatter, O., Kratky, O., Eds.; Academic Press: London, 1982; p 17.
(53) Vonk, C. G.; Kortleve, G. *Kolloid Z. Z. Polym.* **1967**, *220*, 19.
(54) Strobl, G. R.; Schneider, M. J. *J. Polym. Sci.: Polym. Phys. Ed.* **1980**, *18*, 1343.
(55) Hosemann, R.; Bagchi, S. N. *Direct Analysis of Diffraction by Matter*; North-Holland Publishing Co.: Amsterdam, 1962.
(56) Maddams, W. F. *Appl. Spectrosc.* **1980**, *34*, 245.
(57) Huo, P. P.; Cebe, P.; Capel, M. *Macromolecules* **1993**, *26*, 4275.
(58) Blundell, D. J.; Osborn, B. N. *Polymer* **1983**, *24*, 953.
(59) Chen, H.-L.; Porter, R. S. *J. Polym. Sci., Part B: Polym. Phys.* **1993**, *31*, 1845.
(60) Bassett, D. C. *CRC Crit. Rev. Solid State Mater. Sci.* **1984**, *12*, 97.
(61) Vaughan, A. S. *Polymer* **1992**, *33*, 2513.
(62) Ivanov, D. A.; Jonas, A. M. *Bull. Am. Phys. Soc.* **1996**, *41*, 446.
(63) Debier, D.; Jonas, A. M.; Legras, R. *J. Polym. Sci.: Polym. Phys.*, in press.
(64) Flory, P. J. *Macromolecules* **1978**, *11*, 1138.
(65) Aharoni, M. *Polymer* **1980**, *21*, 21; Bianchi, E.; Ciferri, A.; Tealdi, A. *Macromolecules* **1982**, *15*, 1268.

MA9711607